Water Practice & Technology

IWA PUBLISHING

Water Practice & Technology Vol 16 No 4, 1224 doi: 10.2166/wpt.2021.055

Development of hollow δ-FeOOH structures for mercury removal from water

Luiz F. O. Maia [a,*], Guilherme Lages[a], Patricia C. C. Ladeira[b], Bruno Lemos Batista[b], Márcia C. S. Faria[a], Luiz C. A. Oliveira[c], Márcio C. Pereira[a] and Jairo Lisboa Rodrigues[a]

[a] Instituto de Ciência, Engenharia e Tecnologia, Universidade Federal dos Vales do Jequitinhonha e Mucuri, Teófilo Otoni, Minas Gerais 39803-371, Brazil

[b] Centro de Ciências Naturais e Humanas, Universidade Federal do ABC, Rua Santa Adélia, 166, Vila São Pedro, Santo André, SP 09210-170, Brazil

[c] Departamento de Química, Universidade Federal de Minas Gerais, Belo Horizonte, Minas Gerais 31270-901, Brazil

*Corresponding author. E-mail: luiz.maia@ifnmg.edu.br

LFOM, 0000-0002-0772-7531

ABSTRACT

δ-FeOOH, a magnetic iron oxyhydroxide, has a significant number of -OH groups on its surface. These provide an attractive platform for heavy metal species in contaminated water, giving it potential as an adsorbent. Its performance can be improved by increasing the number of active surface sites. δ-FeOOH hollow structures were synthesized on a mesoporous silica surface then treated with NaOH solution. X-ray diffraction (XRD) and transmission electron microscopy (TEM) confirmed that structure synthesis was successful. δ-FeOOH, 5,27 nm, hollow crystals were produced with 63 $m^2\ g^{-1}$ surface area and 20 nm average pore size. The point of zero charge was 4.72, which is beneficial for Hg(II) adsorption near neutral pH. The maximum Hg(II) adsorption capacity at pH 7 was determined as 89.1 $mg\ g^{-1}$. The kinetics data were best fitted by a pseudo-second-order model with k_2 equal 0,1151 $g\ mg^{-1}\ min^{-1}$. Finally, a nanomaterial filter was developed and used to remove mercury in water samples from a Brazilian river.

Key words: adsorption, FeOOH, hollow structures, mercury

HIGHLIGHTS

- δ-FeOOH hollow structures were prepared on a mesoporous silica surface using simple chemical treatment.
- The δ-FeOOH hollow structures are an effective Hg(II) adsorbent.
- The adsorbent had good anti-interference ability to co-existing anions and cations.
- A filter made from the adsorbent treated water effectively from a Brazilian river.

INTRODUCTION

Mercury (Hg) is one of the most toxic metals that can affect human health, due to its volatility, persistence, and bioaccumulation (Yu *et al.* 2016). Severe damage to the nervous system, kidneys, and other organs has been reported after Hg exposure (Shen *et al.* 2014). Thus, there is great concern about the release of mercury into the environment; for example, through mining, and/or urban and industrial waste disposal (Ahamad *et al.* 2017). Among the main chemical forms of Hg, inorganic Hg(II) species in water pose a serious threat because of their mobility and complexity, showing features of wide distribution, low concentration and difficulty in control (Santana *et al.* 2016).

The US Environmental Protection Agency (USEPA), and WHO have set/recommended maxima of 1 μg-Hg L^{-1} for water and 5 μg-Hg L^{-1} for wastes discharged to the environment (Homayoon *et al.* 2017). In recent years, various techniques have been used to remove Hg(II) from water, including solvent extraction, precipitation, coagulation, ion-exchange, reverse osmosis, membrane separation, coagulation, and photoreduction (AlOmar *et al.* 2017). Adsorption is considered an efficient and low cost technique for Hg (II) removal from wastewater effluents (Burakov *et al.* 2018).

Iron oxyhydroxide (FeOOH) nanoparticles are cheap, harmless and eco-friendly (Patra & Kim 2017), and used widely for efficient removal of various metals from aqueous media (Kokkinos *et al.* 2015). Iron hydroxides have been used widely as decontaminants to remove oxyanions like arsenite, arsenate, chromate, vanadate, phosphate, etc (Davantès *et al.* 2016). Recently, δ-FeOOH, magnetic iron oxyhydroxide, has been reported as an efficient

adsorbent for Hg(II) from contaminated water (Maia *et al.* 2019). The maximum Hg(II) adsorption capacity of δ-FeOOH at pH 7 was determined as 35 mg g^{-1}. δ-FeOOH has a significant number of -OH groups on its surface, providing an attractive platform for coordination with Hg(II) metal species. Thus, to pursue high adsorptive performance, it was interesting to increase the number of active surface hydroxyl groups on it.

In this work, δ-FeOOH hollow structures were synthesized on a mesoporous silica surface, which was then treated with NaOH to dissolve the silica. The δ-FeOOH hollow structures were characterized by X-ray diffraction (XRD), transmission electron microscopy (TEM), BET specific surface and zeta potential. The effect of variables on Hg(II) adsorption was investigated and the material was used to treat mercury-contaminated water from the Doce River, Governador Valadares, Minas Gerais, Brazil.

METHODS

Chemicals

$(NH_4)_2Fe(SO_4)_2.6H_2O$ (CAS: 7783-85-9), NaOH (CAS: 1310-73-2), H_2O_2 30% (w/w) (CAS:7722-84-1), and cetyltrimethylammonium bromide (CTAB) (CAS: 57-09-0) were purchased from Vetec (Brazil). Sigma-Aldrich supplied $HgCl_2$ (CAS 7487-94-7) and tetraethyl orthosilicate (TEOS) (CAS: 78-10-4). All chemicals were of analytical grade and used as supplied. The samples and standards were prepared using ultrapure water with a resistivity of 18.2 MΩ cm, which was obtained from a Thermo Scientific Barnstead™ Nanopure™ water purification system.

Synthesis of mesoporous silica (MCM)

The mesoporous silica was synthesized as by Coelho *et al.* (2013) reported by dissolving 1.63 g of CTAB in a mixture of 30 mL of ultrapure water and 10 mL of 1 mol L^{-1} NaOH, adding 3.7 ml of TEOS and stirring the mixture for 24 hours at pH 11. After the contact time, the white precipitate was collected by centrifugation and washed several times until the pH of the final wash was 7. The material obtained was dried in a vacuum desiccator at ambient temperature for 48 hours. To remove the CTAB, 1,0 g of the dried solid was calcined in a muffle furnace at 550 °C for 5 hours.

Synthesis of δ-FeOOH hollow structures

MCM (1.0 g) was dispersed into 50 mL of 0.3 mol L^{-1} of Fe^{2+} solution and sonicated for 5 minutes. Fe^{2+} was precipitated as a green rust in the presence of MCM with 50 mL of 2 mol L^{-1} NaOH, after which 10 mL of 30% H_2O_2 was added immediately, with stirring. Stirring continued for 30 minutes. The reddish brown precipitate FeOOH/MCM formed was washed several times with deionized water and dried in a vacuum desiccator at room temperature.

δ-FeOOH hollow structures were prepared by dissolving 1.0 g of δ-FeOOH/MCM in 50 mL of 5 mol L^{-1} NaOH and stirring at room temperature for 2 hours. Finally, the yellowish-brown material obtained was washed three times with deionized water and dried in a vacuum desiccator.

Materials characterization

Powder X-ray diffraction (XRD) data were collected from 5 to 80° 2θ at a step width of 0.02°, 0.6 s per step, using Cu-Kα ($\lambda = 1.540560$ Å) radiation in a Rigaku Geigerflex diffractometer equipped with a graphite diffracted-beam monochromator. Silicon was used as the external standard. Morphology analyses were conducted with a JEOL JEM 2000EXII transmission electron microscope. The specific surface of the nanoparticles was determined by the BET method, using N_2 adsorption/desorption in an Autosorb 1 Quantachrome instrument and the Barrett-Joyner-Halenda (BJH) method to determine the pore diameter distribution (Barrett *et al.* 1951). The zeta potential was measured by dynamic light scattering (Zetasizer Nano ZS, Malvern, UK). OriginPro (OriginPro, Student Version, 2021) software was used for data processing.

Adsorption experiments

Hg(II) adsorption was investigated by batch method studies to examine the effect of various parameters – pH, contact time, initial Hg(II) concentration, and interferents – and determine the conditions leading to maximum Hg(II) sorption capacity. All experiments were carried in duplicate at 25 $\pm$ 0.1 °C in 50 ml, metal free tubes metal stirred at 200 rpm, using 10 mg of adsorbent. The effect of pH on Hg(II) adsorption was investigated at pH = 3, 5, 7, 9 and 11.

The Hg(II) adsorption rate was determined by batch experiments with varying reaction times. Solutions were in contact with hollow δ-FeOOH nanoparticles for a period of time between 0 and 360 minutes. Adsorption isotherms were obtained by varying the initial Hg(II) concentration in the range 0–40 mg/L. The effect of interferent anions on Hg(II) removal from solution was investigated by performing adsorption experiments in the presence of solutions containing 0 and 50 mg L^{-1} of Cl^-, NO_3^-, SO_4^{2-}, PO_4^{3-}. Binary mixtures of Hg^{2+} ions with different Cu^{2+}, Co^{2+}, Cd^{2+}, Zn^{2+}, Ni^{2+}, Na^+ or Mg^{2+} metals in 0.1 mg L^{-1} concentration were investigated to determine the adsorption capacity of hollow δ-FeOOH in the presence of competitive cations. The initial and residual concentrations of mercury were determined with an inductively coupled plasma mass spectrometer (ICP-MS) (Perkin Elmer NexIon 300D). The analytical conditions are summarized in Table 1.

Table 1 | NexION 300D ICP-MS analysis conditions

Parameter	Value
Nebulizer	Meinhard® concentric glass
RF power	1,300 W
Plasma (gas flow)	15 L min^{-1}
Nebulizer (gas flow)	0.95 L min^{-1}
Auxiliary gas flow	1,2 L min^{-1}
CeO/Ce	0,011
Ba^{++}/Ba^+	0,016
Dwell time	500 ms
Isotope used	^{202}Hg
Replicas	3
Operation mode	Pattern

All samples analyzed after adsorption were submitted to dilution in 2% (v/v) nitric acid (HNO_3), using the USEPA 200.8 protocol and the Hg detection limit was determined as 2 ng L^{-1} (Ewa & Bosnak 2012). The Hg(II) removal efficiency and adsorption capacities were calculated using Equations (1) and (2):

$$q_t = \frac{V(C_i - C_f)}{m} \quad (1)$$

$$\%R = \left(\frac{C_i - C_f}{C_i}\right) \times 100\% \quad (2)$$

where R represents the Hg(II) removal efficiency (%), qt the mercury adsorption capacity on the adsorbent (mg g^{-1}) at a given time, V and m the solution volume (L) and mass of adsorbent (g) respectively, and C_i and C_f the initial and final concentrations of Hg(II) in solution (mg L^{-1}) respectively.

Sample collection

The water contaminated with mercury was collected in Governador Valadares, Minas Gerais, Brazil, in November 2015, using the procedure adopted by Environmental Company of the State of São Paulo (CETESB or Environmental Company of the State of São Paulo) (CETESB 2011). The samples were collected at two sites on the Doce River: P1 is within the area serviced by the water and sewage treatment system at 18°52′55.31 (S) 41°57′.86″ (W) and P2, on the urban perimeter, is at 18°51′22.54 (S) 41°56′10.55″ (W).

Nanofilter development

A nano-adsorbent filter was developed using the procedure reported by Maia *et al.* (2019) to remove mercury from water. 5 mL of a standard solution containing 50 μg-Hg(II) L^{-1} was applied to each filter, which then drained by gravity. The filtrate was collected after 20 minutes of continuous flow.

RESULTS AND DISCUSSION

Characterization of δ-FeOOH hollow structures

The XRD patterns of the synthesized samples are shown in Figure 1. A broadening peak, centered around $2\theta = 23.5°$, corresponds to amorphous silica (Coelho *et al.* 2013; Xiong *et al.* 2017) – Figure 1(a). As shown in Figure 1(a), all diffraction peaks in the XRD patterns can be readily indexed to the phase of δ-FeOOH (JCPDS Card no. 13-87). Figure 1(b) shows a decrease in the peak intensity for amorphous silica, indicating that some of it was removed in treatment with NaOH. The average particle size was calculated using the Scherrer Equation (3) – for the most intense peak (100).

$$D_{hkl} = \frac{0.94\lambda}{\beta\cos\theta} \tag{3}$$

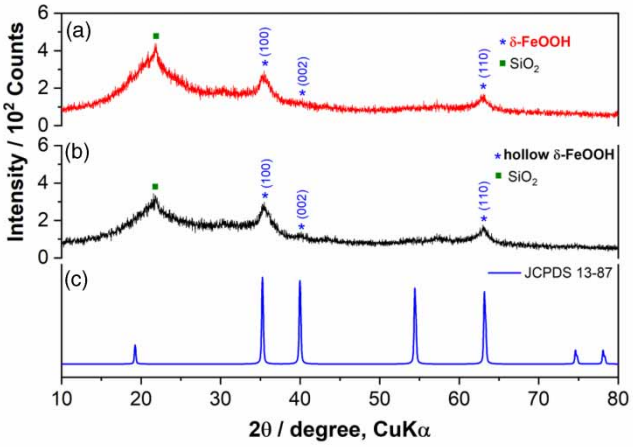

Figure 1 | (a) XRD diffraction pattern of δ-FeOOH/MCM; (b) hollow δ-FeOOH and (c) JCPDS card 13-87.

where 0.94 is the value assigned to the constant 'K', λ is the X-ray wavelength, θ half the diffraction angle, and β the angular width (radians) at the half-maximum intensity. The average crystal sizes calculated before and after treatment were 5.23 and 5.27 nm, respectively.

The TEM image for the δ-FeOOH/MCM hybrid in Figure 2(a) shows a nanoparticle agglomerate, with a clear contrast between the dark δ-FeOOH and pale amorphous SiO_2 that can be seen. It is impossible to define a characteristic form. The δ-FeOOH hollow structures were obtained by treating δ-FeOOH/MCM with 5 mol L^{-1} NaOH to remove the silica. It is possible from the STEM image (Figure 2(b)) to infer the formation of cavities on the nanoparticle surfaces, confirming that much of the nanomaterial has a hollow interior.

The N_2 adsorption–desorption isotherms for the δ-FeOOH/MCM and hollow δ-FeOOH are shown in Figure 3. The isotherms exhibit high N_2 adsorption, reaching 170 and 156 $cm^3\ g^{-1}$ at $p/p_0 = 0.95$ for δ-FeOOH/MCM and hollow δ-FeOOH, respectively. A type IV isotherm was exhibited, characteristic of mesoporous materials, and a type H3 hysteresis loop, which is related to the filling of the mesopores due to capillary condensation. The BET area decreased from 94 $m^2\ g^{-1}$ in δ-FeOOH/MCM to 63 in hollow δ-FeOOH. This occurred because part of the silica was removed in the treatment with NaOH. The pore size distribution (Figure 3, inset) calculated from the desorption branch of the N_2-isotherms by the BJH method, showed an average pore size of 20 nm, thus confirming the presence of mesopores.

Effect of pH

The effect of pH on Hg(II) adsorption onto hollow δ-FeOOH is shown in Figure 4(a). As the pH increased up to 9, mercury adsorption also increased. However, at pH 11, there was a slight decrease. The Hg(II) adsorption capacity at pH 9 was 8.01 mg g^{-1} corresponding to a removal efficiency of 93.3%. Subsequent studies at pH 7 showed Hg(II) removal efficiency of 92.4%.

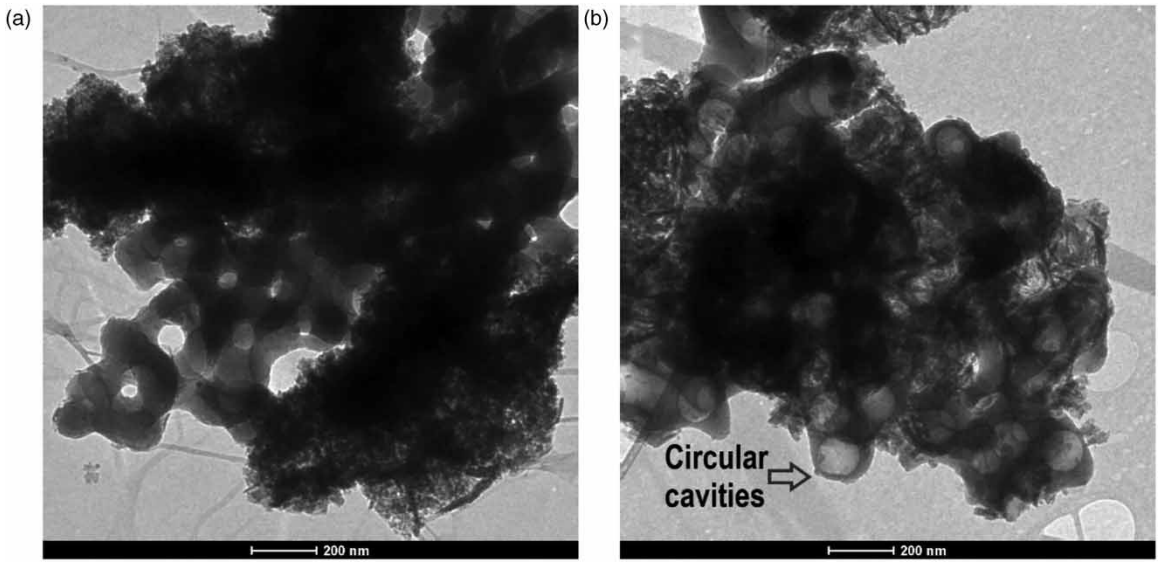

Figure 2 | TEM images (a) δ-FeOOH/MCM and (b) hollow δ-FeOOH.

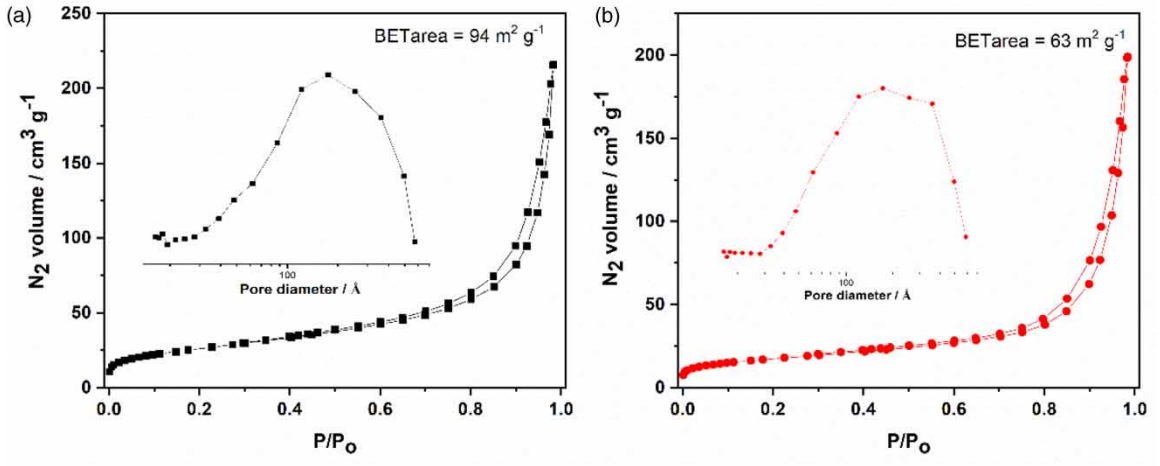

Figure 3 | N_2 adsorption–desorption isotherms and the corresponding pore-size distribution curves (inset) for (a) δ-FeOOH/MCM and (b) hollow δ-FeOOH.

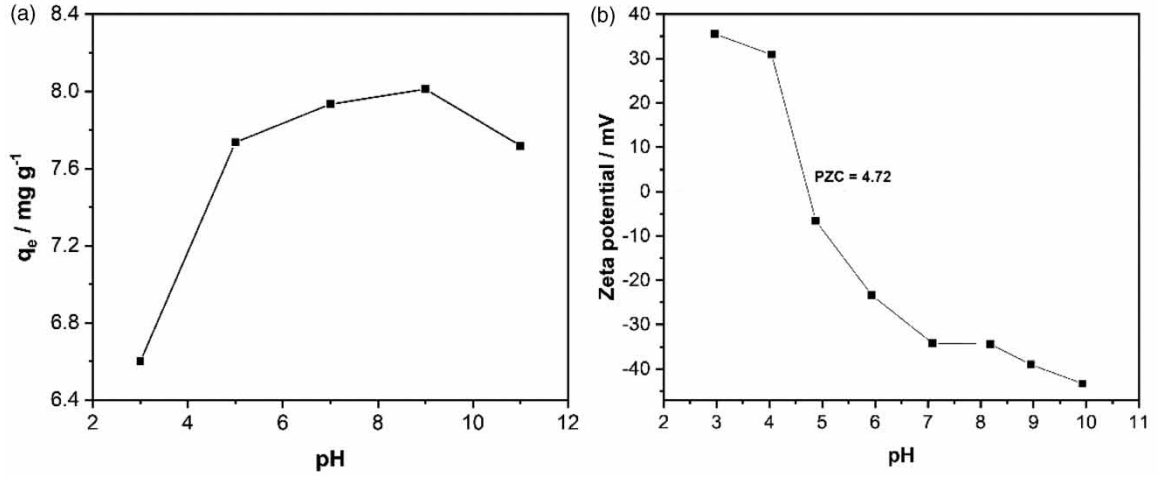

Figure 4 | (a) Effect of pH on Hg(II) adsorption onto hollow δ-FeOOH. Initial $[Hg^{2+}] = 5.0$ mg L^{-1}; adsorbent dose = 0.5 g L^{-1}, shaking speed = 200 rpm; temperature = 25.0 $\pm$ 0.1 °C, and (b) zeta potential measurement for hollow δ-FeOOH.

The change in solution pH results in the formation of different aqueous Hg(II) species, including Hg^{2+}, $HgOH^{+}$, and $Hg(OH)_2$ (Lu *et al.* 2014), and different hollow δ-FeOOH surface charges. When the mercury solution pH is below the point of zero charge (PZC) of hollow δ-FeOOH (PZC = 4.72, Figure 4(b)), the surface of hollow δ-FeOOH is positively charged and interacts very weakly with mercury cations, due to protonation of the surface functional groups, and competition between the mercuric and H^{+} ions present in the solution (Husnain *et al.* 2016). On the other hand, when pH exceeded the PZC, the hollow δ-FeOOH surface was negatively charged and more functional groups were available for metal cation binding due to deprotonation, resulting in electrostatic attraction between Hg(II) and hollow δ-FeOOH. At pH above 9, insoluble metal hydroxide species ($Hg(OH)_2$) are formed, lowering adsorption efficiency (Shen *et al.* 2014).

Adsorption kinetics

The kinetics of Hg(II) adsorption are shown in Figure 5(a). Preliminary studies on the rate of mercury removal by hollow δ-FeOOH at pH 7 indicated that some 89.7% of the total mercury was removed after 60 minutes' adsorption, suggesting that Hg(II) adsorption on hollow δ-FeOOH is rapid initially but decreases gradually with time. Subsequently, the amount adsorbed increased slightly, and a maximum removal efficiency of 91.7% (8.13 mg g^{-1}) was determined. This could arise from the high specific surface of δ-FeOOH due to its small particle size.

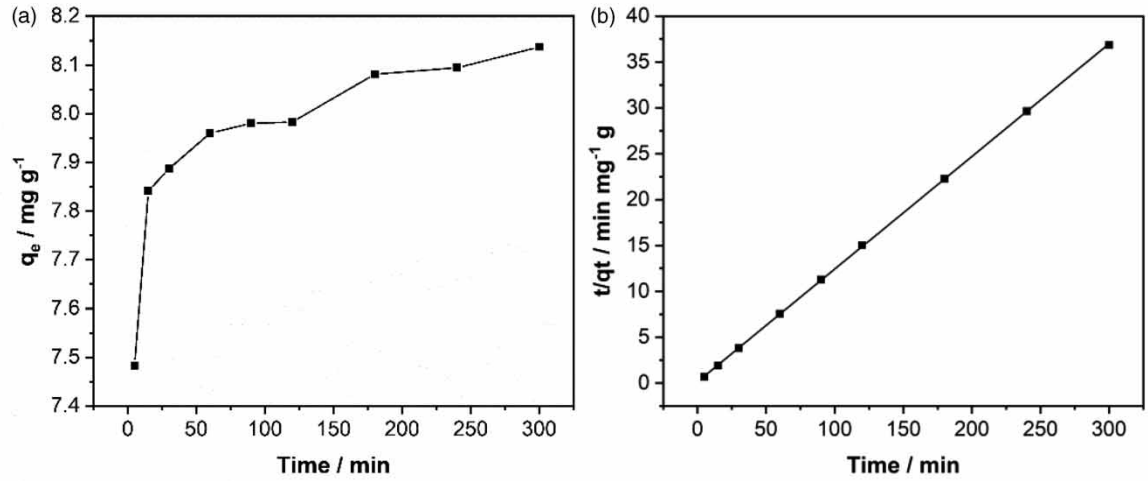

Figure 5 | (a) Hg(II) adsorption kinetics on hollow δ-FeOOH nanoparticles, and (b) pseudo-second-order model. Initial $[Hg^{2+}]$ = 5.0 mg L^{-1}; adsorbent dose = 0.5 g L^{-1}, pH = 7.0 ± 0.3; temperature = 25.0 ± 0.1 °C; shaking speed = 200 rpm.

The pseudo-second-order equation (Equation (4)) was used to fit the experimental data to investigate the adsorption mechanism.

$$\frac{t}{q_t} = \frac{1}{q_e}t + \frac{1}{k_2 q_e^2} \tag{4}$$

where q_t and q_e are the amounts of Hg(II) adsorbed at time t and equilibrium, respectively (mg g^{-1}), and k_2 the rate constant of the pseudo-second-order adsorption (g mg^{-1} min^{-1}).

The linear plot of t/q_t versus t is shown in Figure 5(a). The correlation coefficient for Hg(II) was 0.999. Moreover, the values of q_e calculated show good agreement with the experimental data (Table 2). Hg(II) adsorption in

Table 2 | Kinetic model parameters for Hg(II) adsorption onto hollow δ-FeOOH nanoparticles

Pseudo-second order kinetic

$q_{e,exp}$ (mg g^{-1})	$q_{e,cal}$ (mg g^{-1})	k_2 (g mg^{-1} min^{-1})	R^2
8.137	8.141	0.1151	0.999

hollow δ-FeOOH can thus be approximated favorably by the pseudo-second-order adsorption model. The value of k_2 was calculated as 0.1151 g mg^{-1} min^{-1} and q_e (calculated) was 8.141 mg g^{-1}.

Adsorption isotherm

The effect of the initial Hg(II) concentration on adsorption capacity was also studied (Figure 6). The value of q_e when the Hg(II) concentration was 1.5 mg L^{-1} was 2.56 mg g^{-1}, showing that the adsorbent is effective in adsorbing Hg(II) even at lower concentrations.

The adsorption mechanism at a given temperature is predicted using an adsorption isotherm (Luo *et al.* 2017).

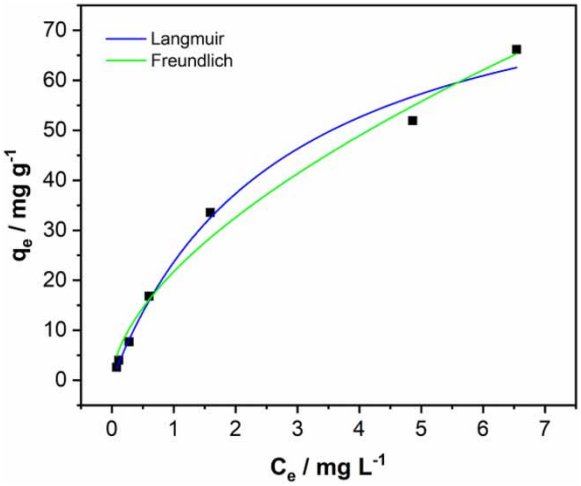

Figure 6 | Adsorption isotherms of Hg(II) onto hollow δ-FeOOH nanoparticles. Initial [Hg^{2+}] = 5.0 mg L^{-1}; adsorbent dose = 0.5 g L^{-1}, pH = 7.0 ± 0.3; temperature = 25.0 ± 0.1 °C; shaking speed = 200 rpm.

The experimental data of mercury adsorption in hollow δ-FeOOH nanoparticles were fitted to the Langmuir and Freundlich isotherm models. The Langmuir model is used for the adsorption process on homogeneous, monolayer surfaces, where adsorption occurs at specific sites on the adsorbent. The Langmuir isotherm is represented by Equation (5):

$$q_e = \frac{k_L Q_m C_e}{1 + k_L C_e} \tag{5}$$

where Q_m (mg g^{-1}) and C_e (mg L^{-1}) are the maximum adsorption capacity and concentration at equilibrium, respectively, and k_L is the Langmuir constant, representing the energy of adsorption (L mg^{-1}).

The Freundlich model is another that is used frequently to describe heterogeneous systems. It is represented by Equation (6):.

$$q_e = k_F C_e^{1/n} \tag{6}$$

where C_e is the equilibrium concentration of the adsorbate (mg L^{-1}), and k_F (L g^{-1}) and 1/n are Freundlich constants representing the adsorption capacity and its intensity, respectively. 1/n values <1.0 indicate an ordinary Langmuir isotherm, whereas a value of 1/n exceeding 1.0 suggests cooperative adsorption. The parameters derived from each model are shown in Table 3. The hollow δ-FeOOH experimental data fit best with the Langmuir model ($R^2 = 0.988$). The Freundlich model showed a slightly lower correlation coefficient ($R^2 = 0.984$), suggesting that Hg(II) adsorption on the hollow structures is monolayer.

The maximum Hg(II) adsorption capacity calculated using the Langmuir model was 89.1 mg g^{-1}, which is higher than that found for δ-FeOOH (Maia *et al.* 2019), possibly due to the increased number of hydroxyl groups (main binding site) in the hollow interior of the nanoparticles. The value of R_L ($=1/(1 + k_L C_0)$) was below 1.0, indicating that the adsorption process was favorable, which was further supported by the 1/n values below 1 in the Freundlich model.

Table 3 | Langmuir and Freundlich isotherm parameters for Hg(II) adsorption

Adsorption isotherm	Parameter	Value	R^2
Langmuir	Q_m (mg g^{-1})	89.1	0.988
	k_L (L mg^{-1})	0.36	
Freundlich	k_F (L g^{-1})	21,69	0.984
	1/n	0.587	

Comparison of adsorption capacity with other adsorbents

The maximum Hg(II) adsorption capacity of hollow δ-FeOOH was compared with that of other iron oxides and hydroxides reported previously in the literature. The 89.1 mg g^{-1} found for hollow δ-FeOOH exceeded those for materials like FeOOH and FeMnOOH (6.4 and 11.9 mg g^{-1}) (Kokkinos *et al.* 2015); Fe_3O_4 and Fe_3O_4@SiO_2 (24.80 and 29.52 mg g^{-1}) (Afraz *et al.* 2017), and Fe-Mn/graphene oxide composite (32.9 mg g^{-1}) (Tang *et al.* 2016), but was lower than the 200 mg g^{-1} found for mesoporous α-FeOOH adsorbent (Patra & Kim 2017), with its high specific surface (152.4 m^2 g^{-1}).

Interference study

Coexisting ions in solution affect many aspects of the adsorption process (Zhou *et al.* 2017). For example, different species can compete for the limited number of active sites, influence electrostatic interactions and impede the ion transfer from solution to the adsorbent surface (Tan *et al.* 2015).

Figure 7(a) shows that Hg(II) adsorption efficiency was affected little by the presence of NO_3^- or SO_4^{2-}. The decrease of about 5% adsorbed mercury in the presence of Cl^- was due to the formation of aqueous Hg(II)-Cl complexes; that is, $HgCl_3^-$ and $HgCl_4^{2-}$ (Shan *et al.* 2015), leading to electrostatic repulsion from the negative surface of hollow δ-FeOOH. With phosphate, the reduction was slightly greater at about 7%, because species formed that have little or no affinity with the variable-charge surfaces (Sarkar *et al.* 2000).

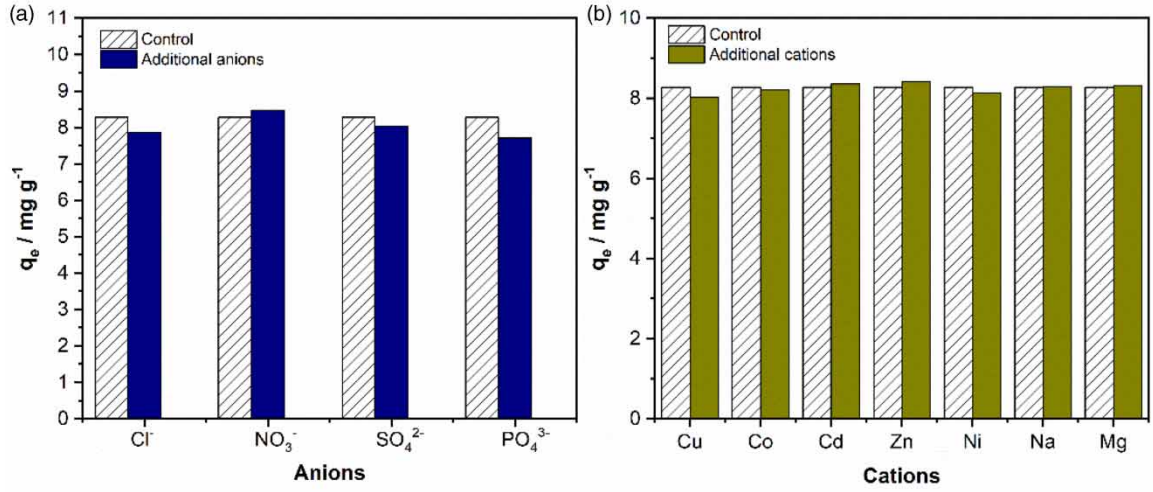

Figure 7 | Hg(II) adsorption capacity in the presence of (a) additional anions and (b) additional cations. Common conditions: Initial $[Hg^{2+}] = 5.0$ mg L^{-1}; adsorbent dose = 0.5 g L^{-1}, pH = 7.0 ± 0.3; temperature = 25.0 ± 0.1 °C; shaking speed = 200 rpm.

Figure 7(b) shows the competitive adsorption of Hg(II) in the presence of various metal ions in water. There was no significant interference in adsorption capacity at the concentration studied.

Application to real samples

The filter containing 0.5 g of hollow δ-FeOOH was tested initially for the treatment of water contaminated with a mercury standard at 50 μg-Hg L^{-1}. After filtration, the concentration was 1.150 μg-Hg L^{-1}, a removal efficiency of 97.7%. Samples of water collected from the Doce River and filtered in the same way contained Hg concentrations below the limit of detection – see Table 4.

Table 4 | Hg determination in real samples

Samples	Hg(II) (μg L^{-1}) ± SD[a] before filtration	Hg(II) (μg L^{-1}) after filtration
P1	29.93 ± 0.062	< LOD[b]
P2	30.14 ± 0.067	< LOD[b]

[a]SD, standard deviation; [b]LOD, Limit of detection.

CONCLUSIONS

Hollow, mesoporous δ-FeOOH structures were fabricated successfully using a simple, eco-friendly method. They are an effective tool for Hg(II) adsorption from aqueous solutions. Studies showed that their efficiency in Hg(II) adsorption is about 92.4% at pH 7.

The results of kinetic tests showed that Hg(II) adsorption was fast, occurring in the first 60 minutes with approximately 90% removal. The material offered high adsorption capacity (89.1 mg g^{-1}) with low interference for Hg(II) removal. The nanomaterial filter produced was efficient in mercury removal from water from the Doce River, lowering the mercury concentration below the maxima recommended by WHO and USEPA.

ACKNOWLEDGEMENTS

The authors are grateful to CNPq, FAPEMIG, Rede Mineira de Química (RQ-MG), and CAPES for the financial support and fellowships.

CONFLICTS OF INTEREST

There are no conflicts to declare.

DATA AVAILABILITY STATEMENT

All relevant data are included in the paper or its Supplementary Information.

REFERENCES

Afraz, A., Hajian, A., Niknam, Z., Mosayebi, E., Yusefi, A. & Sillanpää, M. 2017 Amin-functionalized magnetic-silica core-shell nanoparticles for removal of Hg^{2+} from aqueous solution. *J. Dispersion Sci. Technol.* **38**, 750. https://doi.org/10.1080/01932691.2016.1193815.

Ahamad, T., Naushad, M., Al-Maswari, B. M., Ahmed, J., ALOthman, Z. A., Alshehri, S. M. & Alqadami, A. A. 2017 Synthesis of a recyclable mesoporous nanocomposite for efficient removal of toxic Hg^{2+} from aqueous medium. *J. Ind. Eng. Chem.* **53**, 268. https://doi.org/10.1016/j.jiec.2017.04.035.

AlOmar, M. K., Alsaadi, M. A., Hayyan, M., Akib, S., Ibrahim, M. & Hashim, M. A. 2017 Allyl triphenyl phosphonium bromide based DES-functionalized carbon nanotubes for the removal of mercury from water. *Chemosphere* **167**, 44. https://doi.org/10.1016/j.chemosphere.2016.09.133.

Barrett, E. P., Joyner, L. G. & Halenda, P. P. 1951 The determination of pore volume and area distributions in porous substances. I. Computations From Nitrogen Isotherms. *J. Am. Chem. Soc.* **73**(1), 373. https://doi.org/10.1021/ja01145a126.

Burakov, A. E., Galunin, E. V., Burakova, I. V., Kucherova, A. E., Agarwal, S., Tkachev, A. G. & Gupta, V. K. 2018 Adsorption of heavy metals on conventional and nanostructured materials for wastewater treatment purposes: a review. *Ecotoxicol. Environ. Saf.* **148**, 702. https://doi.org/10.1016/j.ecoenv.2017.11.034.

Coelho, J. V., Guedes, M. S., Barrera, D., Sapag, K., Pereira, M. C. & Oliveira, L. C. A. 2013 Controlling the morphology and pore size of mesostructured silica nanoparticles: the role of the iron oxidation state. *Dalton Trans.* **42**, 11271. https://doi.org/10.1039/c3dt50794 g.

Davantès, A., Costa, D. & Lefèvre, G. 2016 Molybdenum(VI) adsorption onto lepidocrocite (γ-FeOOH): in situ vibrational spectroscopy and DFT + U theoretical study. *J. Phys. Chem. C.* **120**, 11871. https://doi.org/10.1021/acs.jpcc.6b00722.

Environmental Company of the State of São Paulo 2011 *National Sample Collection and Preservation Guide: Water, Sediment, Aquatic Communities and Liquid Effluents*. Available from: http://www.cetesb.sp.gov.br (accessed 10 October 2015).

Ewa, P. & Bosnak, C. 2012 The analysis of drinking waters by USEPA method 200.8 using the NexION 300D/350D ICP-MS in standard, collision and reaction modes. PerkinElmer. Inc 940:1–9, Shelton, CT USA. Available from: https://www.perkinelmer.com/CMSResources/Images/44-134580APP_NexION300D-US-EPA200-8-Drinking-Water.pdf. (accessed 5 Ago 2017).

Homayoon, F., Faghihian, H. & Torki, F. 2017 Application of a novel magnetic carbon nanotube adsorbent for removal of mercury from aqueous solutions. *Environ. Sci. Pollut. R.* **24**, 11764. https://doi.org/10.1007/s11356-017-8780-4.

Husnain, S. M., Kim, J.-H., Lee, C.-S., Chang, Y.-Y., Um, W. & Chang, Y.-S. 2016 Superparamagnetic nalidixic acid grafted magnetite (Fe_3O_4/NA) for rapid and efficient mercury removal from water. *RSC Adv.* **6**, 35825. https://doi.org/10.1039/C5RA25927D.

Kokkinos, E., Simeonidis, K., Zouboulis, A. & Mitrakas, M. 2015 Mercury removal from drinking water by single iron and binary iron-manganese oxyhydroxides. *Desalin. Water Treat.* **54**, 2082. https://doi.org/10.1080/19443994.2014.934105.

Lu, X., Huangfu, X. & Ma, J. 2014 Removal of trace mercury(II) from aqueous solution by in situ formed Mn-Fe (hydr)oxides. *J. Hazard. Mater.* **280**, 71. https://doi.org/10.1016/j.jhazmat.2014.07.056.

Luo, H., Zhang, S., Li, X., Liu, X., Xu, Q., Liu, J. & Wang, Z. 2017 Tannic acid modified Fe_3O_4 core–shell nanoparticles for adsorption of Pb^{2+} and Hg^{2+}. *J. Taiwan Inst. Chem. Eng.* **72**, 163. https://doi.org/10.1016/j.jtice.2017.01.026.

Maia, L. F. O., Hott, R. C., Ladeira, P. C. C., Batista, B. L., Andrade, T. G., Santos, M. S., Faria, M. C. S., Oliveira, L. C. A., Monteiro, D. S., Pereira, M. C. & Rodrigues, J. L. 2019 Simple synthesis and characterization of L-Cystine functionalized (-FeOOH for highly efficient Hg(II) removal from contaminated water and mining waste. *Chemosphere* **215**, 422. https://doi.org/10.1016/j.chemosphere.2018.10.072.

OriginPro, Student Version 2021; OriginLab Corporation: Northampton, MA, USA, 2021.

Patra, A. K. & Kim, D. 2017 Smart design of self-assembled mesoporous α-FeOOH nanoparticles: high-surface-area sorbent for Hg^{2+} from wastewater. *ACS Sustainable Chem. Eng.* **5**, 1272. https://doi.org/10.1021/acssuschemeng.6b00937.

Santana, A. J., Dos Santos, W. N. L., Silva, L. O. B. & Virgens, C. F. 2016 Removal of mercury(II) ions in aqueous solution using the peel biomass of *Pachira aquatica* Aubl: kinetics and adsorption equilibrium studies. *Environ. Monit. Assess.* **188**, 293. https://doi.org/10.1007/s10661-016-5266-7.

Sarkar, D., Essington, M. E. & Misra, K. C. 2000 Adsorption of mercury(II) by kaolinite. *Soil Sci. Soc. Am. J.* **64**, 1968. https://doi.org/10.2136/sssaj2000.6461968x.

Shan, C., Ma, Z., Tong, M. & Ni, J. 2015 Removal of Hg(II) by poly(1-vinylimidazole)-grafted Fe_3O_4 at SiO_2 magnetic nanoparticles. *Water Res.* **69**, 252. https://doi.org/10.1016/j.watres.2014.11.030.

Shen, X., Wang, Q., Chen, W. & Pang, Y. 2014 One-step synthesis of water-dispersible cysteine functionalized magnetic Fe_3O_4 nanoparticles for mercury(II) removal from aqueous solutions. *Appl. Surf. Sci.* **317**, 1028. https://doi.org/10.1016/j.apsusc.2014.09.033.

Tan, P., Sun, J., Hu, Y., Fang, Z., Bi, Q., Chen, Y. & Cheng, J. 2015 Adsorption of Cu^{2+}, Cd^{2+} and Ni^{2+} from aqueous single metal solutions on graphene oxide membranes. *J. Hazard. Mater.* **297**, 251. https://doi.org/10.1016/j.jhazmat.2015.04.068.

Tang, J., Huang, Y., Gong, Y., Lyu, H., Wang, Q. & Ma, J. 2016 Preparation of a novel graphene oxide/Fe-Mn composite and its application for aqueous Hg (II) removal. *J. Hazard. Mater.* **316**, 151. https://doi.org/10.1016/j.jhazmat.2016.05.028.

Xiong, L., Huang, X., Liu, Y. & Pan, L. 2017 One-step preparation and characterization of core-shell SiO_2/Ag composite spheres by pulse plating. *Sci. Eng. Compos. Mater.* **24**, 423. https://doi.org/10.1515/secm-2015-0227.

Yu, J.-G., Yue, B.-Y., Wu, X.-W., Liu, Q., Jiao, F.-P., Jiang, X.-Y. & Chen, X.-Q. 2016 Removal of mercury by adsorption: a review. *Environ. Sci. Pollut. R.* **23**, 5056. https://doi.org/10.1007/s11356-015-5880-x.

Zhou, C., Zhu, H., Wang, Q., Wang, J., Cheng, J., Guo, J., Zhou, X. & Bai, R. 2017 Adsorption of mercury(ii) with an Fe_3O_4 magnetic polypyrrole – graphene oxide nanocomposite. *RSC Adv.* **7**, 18466. https://doi.org/10.1039/c7ra01147d.

Received 13 April 2021; accepted in revised form 3 June 2021. Available online 16 June 2021